Solar Energy 197 (2020) 266–278

Contents lists available at ScienceDirect

Solar Energy

journal homepage: www.elsevier.com/locate/solener

Errors in PV power modelling due to the lack of spectral and angular details of solar irradiance inputs

N. Lindsay[a], Q. Libois[a,*], J. Badosa[b], A. Migan-Dubois[c], V. Bourdin[d]

[a] CNRM, Université de Toulouse, Météo-France, CNRS, 42 Avenue Gaspard Coriolis, Toulouse 31100, France
[b] LMD, IPSL, École Polytechnique, Université Paris-Saclay, ENS, PSL Research University, Sorbonne Université, CNRS, Route de Saclay 91128 Palaiseau, France
[c] GeePs – Laboratoire Génie électrique et électronique de Paris, CNRS, SUPELEC, UPMC, University Paris-Sud 11, 11 rue Joliot-Curie, Plateau de Moulon, 91192 Gif-sur-Yvette Cedex, France
[d] LIMSI – Laboratoire d'Informatique pour la Mécanique et les Sciences de l'Ingénieur, CNRS, Rue John von Neumann, 91405 Orsay Cedex, France

ARTICLE INFO

Keywords:
PV power
PV module performance
Cloud–radiation interactions
Spectral irradiance
Numerical weather prediction

ABSTRACT

Photovoltaic (PV) modules are sensitive to the spectral distribution of solar irradiance. Although numerical weather prediction (NWP) models compute irradiance in several spectral bands, only broadband quantities are provided in the standard outputs used for PV forecasts. This study investigates how this lack of information impacts PV power estimation. A physical PV model is first designed that accounts for the spectral distribution of irradiance and the spectral response of the panels. This model is evaluated using measurements performed at Site Instrumental de Recherche par Télédétection Atmosphérique (SIRTA), Palaiseau, France. The mean relative difference between simulated and measured PV power for a monocrystalline silicon module of 250 W nominal power is −0.9%, and the mean bias is −2.0 W. This model is then used to investigate the impact of solar zenith angle and clouds on the performance of PV modules. PV performance can increase in cloudy conditions by 5% through spectral filtering of near-infrared irradiance, and by 18% when only the useful irradiance is considered to compute performance. This spectral effects is not captured by the PV model when only broadband irradiances are used. In such case errors up to 15% are obtained in simulated PV power compared to using a state-of-the-art NWP model providing irradiance in 14 spectral bands. More generally, broadband global horizontal irradiance appears insufficient for accurate PV power modelling, highlighting the added value of spectrally-and-angularly-refined irradiances. This stresses that PV models should use more detailed irradiance inputs, which could be easily achieved by exploiting internal variables of NWP models.

1. Introduction

Solar energy is characterised by large temporal fluctuations, in particular because it is sensitive to the presence and characteristics of clouds (Antonanzas et al., 2016). This variability is detrimental to the stability of the electricity grid, making the integration of solar energy at large scales challenging (e.g. Antonanzas et al., 2016). Correctly predicting the photovoltaic (PV) production of a solar farm at various time scales is thus a topical issue and has lead to the development of a number of PV power forecast models which aim at computing PV power from weather forecasts (e.g. De Soto et al., 2006; King et al., 2004). These models can be either statistical or physical (Kostylev and Pavlovski, 2011; Diagne et al., 2013; Das et al., 2018), and this study focuses on physical PV models. In a physical model, all physical processes involved in the conversion of solar irradiance into electric power are successively modelled. This includes transposition (converting the solar irradiance on a horizontal surface into plane-of-array (POA) irradiance), optical losses, temperature variations of the PV cells and their electrical response to the cell-impacting irradiance. The influence of temperature is significant, with typically a power reduction of 0.2% to 0.5% per degree difference from 25 °C for crystalline solar cells (Mittag et al., 2019), and has been widely studied. It is nowadays commonly accounted for in PV models (e.g. King et al., 2004; Skoplaki et al., 2008). However, the PV cells constituting the module are also sensitive to the spectral distribution of solar irradiance, as only sufficiently energetic photons generate current. This has motivated studies (e.g. Marion, 2012; Stark and Theristis, 2015) on the impact of air mass, aerosol optical depth and precipitable water – all affecting the spectral properties of radiation – on the performance of PV cells, hereafter defined as the ratio of PV power to POA irradiance. For instance, direct and diffuse radiation in clear sky conditions are known to result in different PV performances (Kirn and Topic, 2017). Likewise, the

* Corresponding author.
E-mail address: quentin.libois@meteo.fr (Q. Libois).

https://doi.org/10.1016/j.solener.2019.12.042
Received 22 October 2019; Received in revised form 3 December 2019; Accepted 15 December 2019

Nomenclature

α	Spectral response correction factor
β	Module inclination
λ	Wavelength
λ_{gap}	Cutoff wavelength
ρ	PV module performance
ρ^*	PV module performance based on the useful POA irradiance
τ	Cloud optical thickness
SR_{ideal}	Ideal spectral response
$SR_{modelled}$	Modelled spectral response
θ_i	Angle of incidence
θ_r	Angle of refraction
a, b, ΔT	Empirical parameters
$C_{T,I_{SC}}$	Short-circuit current temperature coefficient
E_λ	Photon energy
E_g	Energy gap
G	Irradiance
g	Asymmetry parameter
G_{ASTM}	Plane-Of-Array Irradiance for the ASTM spectrum
G_{POA}	Plane-Of-Array Irradiance
G_{ref}	Reference spectrum
G_{STC}	STC reference spectrum
G_c	Cell-impacting irradiance
I_0	Reverse saturation current
I_{SC}	Short-circuit current
I_D	Photodiode current
I_L	Photogenerated current
k	Boltzmann constant
n_0	Index of refraction of air
n_1	Index of refraction of glass
P	Power
P_{MPP}	Maximum power
q	Elemental charge
R_s	Series resistance
R_{sh}	Shunt resistance
T_{mod}	Module temperature
T_a	Ambient temperature
T_c	Cell temperature
T_g	Transmittance of the global irradiance
U	Wind speed
V	Load voltage
V_{OC}	Open-circuit voltage
V_t	Thermal voltage
APE	Average Photon Energy
ASTM	American Society for Testing and Materials
c	Speed of light
DC	Direct Current
ECMWF	European Center Range Weather Forecast
FF	Fill Factor
GHI	Global Horizontal Irradiance
h	Planck constant
MM	Spectral mismatch factor
MRE	Mean Relative Error
NOCT	Nominal Operating Cell Temperature
NWP	Numerical Weather Prediction
OL	Optical Losses
POA	Plane-Of-Array
PV	Photovoltaic
SAA	Solar Azimuth Angle
SR	Spectral Response
STC	Standard Test Conditions
SW	Short-Wave
SZA	Solar Zenith Angle
TOA	Top-Of-Atmosphere
UF	Useful Fraction
USSA	US Standard Atmosphere

increase in PV performance under cloudy skies due to the shift of the spectrum towards the blue domain has been documented (e.g. Jardine et al., 2001; Nofuentes et al., 2014). These “spectral effects” have thus been observed for various technologies, locations, and seasons during observations campaigns (King et al., 1997; Jardine et al., 2001; Gottschalg et al., 2004; Ghitas, 2012; Dirnberger et al., 2015), but they are not always properly accounted for in PV models.

Indeed, despite the recognized importance of the spectral effects (e.g. Nofuentes et al., 2017), PV models generally rely on variables provided by atmospheric models which only include broadband irradiance (i.e. integrated over the full short-wave (SW) domain). Consequently, the spectral distribution of the incident irradiance is unknown and the spectral effects are either neglected (e.g. Jerez et al., 2015) or accounted for through *ad hoc* correction factors (e.g. King et al., 2004). Spectral effects have thus been investigated via the average photon energy (APE) (Dirnberger et al., 2015), the useful fraction (UF) (Gottschalg et al., 2003), or the spectral mismatch factor (MM) (Nofuentes et al., 2014; Stark and Theristis, 2015; Dirnberger et al., 2015). However these quantities are not available from common weather products. Even more critically, atmospheric models sometimes only provide the global horizontal irradiance (GHI), in which case the partition between direct and diffuse is unspecified and also has to be parameterized (e.g. Gueymard and Ruiz-Arias, 2016).

Yet atmospheric models handle spectral irradiances as internal variables, which could be valuable for PV applications. This spectral information is not usually output because atmospheric models resort to spectral bands only as an intermediate step to increase the accuracy of the broadband radiative budgets of the atmosphere and surface (e.g. RRTM, Mlawer et al., 1997). Similarly, the direct and diffuse components of radiation are internally computed, though they are rarely output. Extracting this spectral and angular information is practically straightforward as no extra computation is involved, and could be beneficial to PV power forecasts. This has for instance motivated the development of the Numerical Weather Prediction (NWP) model WRF-SOLAR (Jimenez et al., 2016).

Based on this observation, the primary objective of this paper is to investigate the benefit of using NWP solar irradiance outputs with detailed spectral and angular information compared to the standard broadband outputs. These benefits are assessed through a particular focus on cloud-radiation interactions and their impact on PV performance because clouds are mostly responsible for changes in spectral distribution. This implies comparing PV estimations obtained from standard outputs –broadband irradiance and sometimes only GHI– on the one hand, and from angularly and spectrally detailed outputs on the other hand. To this end, a dedicated physical PV model is developed that converts solar energy into electrical energy. It is similar to existing models in most respects, but includes a novel treatment of the spectral distribution of solar irradiance (Section 3). To validate this model, simulated PV power computed from GHI measurements are compared to PV power measurements made at the SIRTA, an atmospheric laboratory 20 km south of Paris, France (Haeffelin et al., 2005). A theoretical sensitivity study is then performed by coupling the PV model with the state-of-the-art 14-band radiative transfer model ecRad (Hogan and Bozzo, 2018), operationally used at the European Center for Medium-Range Weather Forecast (ECMWF). To investigate the impact of the spectral and angular information of input irradiance in cloudy conditions, ecRad simulations are performed for ideal overcast conditions with homogeneous clouds and various solar zenith angles (SZA), and

the corresponding surface irradiances fed into the PV code. To study the impact of the spectral resolution, the spectral outputs of ecRad are merged in order to virtually degrade the spectral information. The impact of angular information is investigated by comparing simulations where only GHI, or both the direct and diffuse irradiances, are provided. The results of these investigations are presented in Section 4. Finally, Section 5 highlights practical consequences of this academic study and provides more perspectives. Before that, however, Section 2 aims at providing some background knowledge about PV power and the effects of clouds on solar radiation.

2. Theoretical background

2.1. Photovoltaic effect

The photocurrent generated by a PV cell is highly dependent on the spectral characteristics of the impinging irradiance. The spectral sensitivity of PV cells is quantified by the spectral response (SR), which is the ratio between the photocurrent and the incident power at a given wavelength. Given that the energy of a photon E_λ is related to its wavelength λ, Planck constant h and the speed of light c:

$$E_\lambda = \frac{hc}{\lambda}, \tag{1}$$

the ideal SR reads:

$$\mathrm{SR}_{\mathrm{ideal}}(\lambda) = \begin{Bmatrix} q\frac{\lambda}{hc}, & \mathrm{if}\lambda < \lambda_{\mathrm{gap}} \\ 0, & \mathrm{otherwise} \end{Bmatrix}, \tag{2}$$

where q is the elemental charge. For a given incident power, the generated current increases linearly with wavelength up to the cutoff wavelength λ_{gap}. Above λ_{gap}, it drops to zero as the photons are no longer energetic enough to excite electrons. The useful irradiance is herafter defined as the integrated irradiance up to λ_{gap}.

2.2. Impact of clouds on solar radiation

Clouds primarily alter PV power by reducing transmitted irradiance at the surface. However, for a given POA irradiance, PV power (or equivalently PV performance) also depends on the spectral and angular distributions of incoming irradiance, which is also altered by clouds. This paper investigates the importance of spectral and angular details of irradiance inputs for PV power modelling through this specific impact of clouds on the performance of PV modules. The transmittance of a homogeneous cloud mostly depends on its optical thickness, single scattering albedo and asymmetry parameter (e.g. Kokhanovsky, 2004). The single scattering albedo mostly depends on the absorption coefficient of liquid water, shown in Fig. 1. It highlights that water absorbs much more radiation in the near-infrared (NIR) than in the visible. This spectral signature is also found in cloud transmittance (Fig. 1), with differences close to 10% across the useful spectral range for a cloud with optical thickness 5. This demonstrates that clouds act as spectral filters. As they mainly absorb those photons that cannot be absorbed by solar cells (e.g. wavelengths above λ_{gap}~1100 nm for c-Si technology), clouds tend to increase PV performance relative to clear sky. In addition, the spectral distribution of irradiance for $\lambda \leqslant \lambda_{\mathrm{gap}}$ will be significantly different under clear and cloudy skies.

Fig. 2 shows the atmospheric transmittance and the partition between direct and diffuse irradiance as a function of cloud optical thickness in a clean (i.e. without aerosols) atmosphere. It shows that the partition is very sensitive to cloud characteristics, especially for optical thicknesses below 20. The distinction between direct and diffuse radiation is critical not only to characterise the angular properties of irradiance, but also its spectral distribution. Indeed, while diffuse radiation in clean and clear conditions mainly comes from Rayleigh scattering, resulting in a distribution peaking in the blue domain, direct radiation is more evenly distributed over the spectrum (Fig. 3). As a consequence, direct radiation is generally slightly more efficient than diffuse radiation for PV power.

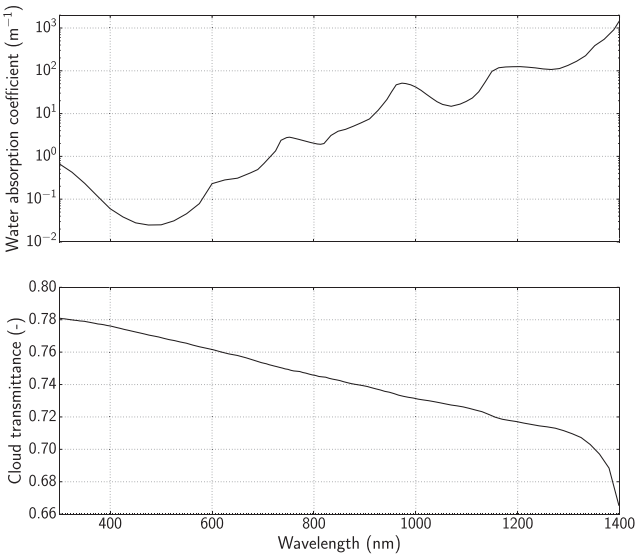

Fig. 1. (top) Absorption coefficient of liquid water computed from the refractive index of Hale and Querry (1973). This database was also used to compute the cloud optical properties in ecRad (Section 3). (bottom) Spectral transmittance of a cumulus cloud of optical thickness 5 computed with ARTDECO (Section 3).

3. Data and methods

3.1. In situ observations dataset

In this study, an exhaustive dataset including atmospheric and PV measurements from SIRTA (Palaiseau, France) over the period January 2015 – June 2017 is used (Badosa et al., 2015) to evaluate the developed PV model. The focus is on a single PV monocrystalline silicon (c-Si) module (France Watts, 250 W nominal power, South-facing with an inclination of 27°), whose operating conditions are monitored (module temperature T_{mod}, and I-V curve characterisation from which the PV maximum power P_{MPP}, the fill factor FF and the open-circuit voltage V_{OC} are derived). Although other technologies with lower λ_{gap} are known to be more sensitive to spectral effects, c-Si technology was chosen for this study because it is widely used and offers good PV performance. GHI and the diffuse horizontal irradiance are measured thanks to a CMP22 Kipp & Zonen Pyranometer and the POA irradiance with a SR01 Hukseflux pyranometer. Wind speed and air temperature are also available. All data are 10-min averaged variables in order to account for the 700 m distance between some of the instruments which could induce inconsistencies at shorter time scales, and to overcome any issues due to differing sampling frequencies between instruments.

3.2. Radiative transfer codes

Two radiation codes are used in this study. ARTDECO[1] is used to compute a set of reference clear-sky spectra at high spectral resolution. These spectra are used in the PV model. ecRad is used for the sensitivity study to clouds because it mimics irradiance outputs of NWP models.

ARTDECO is a versatile and user-friendly radiative transfer model recently developed at Laboratoire d'Optique Atmosphérique (Lille, France) by the French atmospheric radiative transfer community (e.g. Frouin et al., 2018). Here it is run at 10 cm^{-1} resolution with a

[1] freely available from http://www.icare.univ-lille1.fr/projects/artdeco.

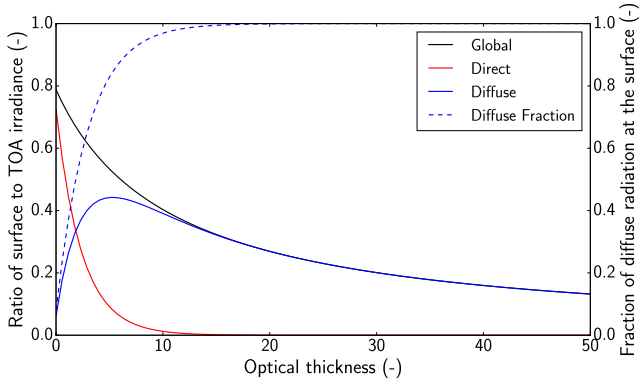

Fig. 2. Atmospheric transmittance (computed as the ratio of surface to Top-Of-Atmosphere (TOA) irradiance), partition into direct and diffuse components (solid lines) and fraction of diffuse radiation at the surface (dashed line) as a function of cloud optical thickness, simulated with ecRad (Section 3) using the US Standard Atmosphere 1976 without aerosols. SZA equals 48° and the sky is overcast by a homogeneous cloud. Note that ecRad uses the δ-Eddington approximation (Joseph et al., 1976) approximation, so that direct radiation includes some radiation that has been forward scattered.

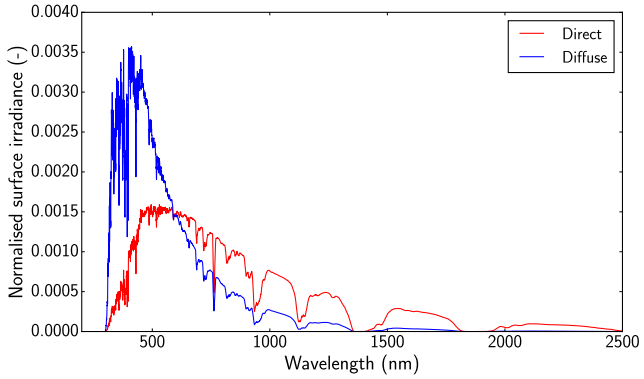

Fig. 3. Clear-sky direct and diffuse solar irradiances, simulated with ARTDECO. The US Standard Atmosphere 1976 without aerosols is used, and SZA = 48.2°. The surface albedo corresponds to vegetation. Both spectra were normalised to have unit integrals.

correlated-*k* distribution and uses the DISORT model (Stamnes et al., 1988) to solve the radiative transfer equation. It is thus similar to libRadtran (Mayer and Kylling, 2005) in terms of capabilities and performances. The reference spectra are computed for atmospheric conditions as close as possible to the standard conditions used to compute the ASTM (American Society for Testing and Materials) solar spectrum G173-03. For this reason, the United States Standard Atmosphere (USSA) 1976 is used. Because the *rural* aerosols profile commonly used to compute the ASTM spectrum is not available in ARTDECO, sulfate aerosols are included in the profile instead. Adding sulfate aerosols at 50% relative humidity from the OPAC database (Hess et al., 1998) with an optical depth of 0.06 at 550 nm allowed to reproduce the standard 1000 W m^{-2} of the ASTM spectrum once projected on the module. This aerosol load is thus used to compute the reference spectra. The surface spectral albedo is set to that of vegetation. The direct and diffuse spectra are computed for a variety of SZAs. In Section 3.3.3, these spectra are used to refine the spectral resolution of irradiance outputs. The high spectral resolution allows to account for the detailed spectral distribution of incident solar radiation, especially around λ_{gap}. Note that the reference spectra could have alternatively been obtained with the SMARTS model (Myers and Gueymard, 2004) or libRadtran.

ecRad is the radiation code implemented in the Integrated Forecast System (IFS) of ECMWF. Here its standalone version is used,[2] meaning that it is fully external to the IFS code and can be used as any other radiative transfer code. ecRad is a two-stream model based on correlated-*k* distributions. Given a vertical description of the atmosphere, it computes SW radiative fluxes in the spectral bands corresponding to those of the Rapid Radiative Transfer Model (RRTM, Mlawer et al., 1997; Morcrette et al., 2008) as detailed in Table 1. RRTM is extensively used in the weather and climate community (e.g. Oreopoulos et al., 2012). All ecRad simulations are performed with the USSA 1976 (Myers et al., 2002) as a background atmosphere. ecRad has the capability to handle aerosols. The latter have to be described in terms of their type, and vertical distribution of mass mixing ratio. Within the IFS, ecRad computations include the aerosols provided by the host model, which vary in space and time. However in the sensitivity study the simulations are performed without aerosols because (1) it seeks at isolating the physical processes related to clouds hence prevents any competition between cloud and aerosols radiative effects; (2) any choice of aerosol vertical distribution and type would have been arbitrary and; (3) the sensitivity study is intentionally an academic exercise. The broadband surface albedo is set to 0.2, a typical broadband value for grassland (e.g. Lohou and Patton, 2014). To study the influence of clouds, a 1-km-thick homogeneous cloud is added to the USSA atmosphere. It is located between 2 and 3 km with droplets effective radius of 10 μm. Its optical thickness, computed after the parameterization of Edwards and Slingo (1996), is varied by varying its liquid water mixing ratio. Although this ideal cloud geometry does not encompass the variety and complexity of natural cloud structures (e.g. multi-layer clouds, broken clouds, thin cirrus clouds), it is consistent with the crude representation of clouds in NWP and climate models, and is often used in theoretical radiative transfer studies (e.g. Nielsen et al., 2014). It will provide a first quantitative assessment of the effect of clouds on PV performance in the framework of NWP models. However an exhaustive assessment of cloud effects on PV power is beyond the scope of this study and would require 3D radiative transfer computations performed on realistic cloud fields, which is far from the capabilities of operational NWP models.

3.3. The photovoltaic model

3.3.1. Overall approach

The developed PV model relies on the "one-diode model" (Fig. 4) as in Lorenzo (2003), assuming a constant series resistance R_s and an infinite shunt resistance R_{sh} (i.e. its effects are neglected). In the following, both power and current are defined per unit area to be consistent with the irradiance provided per unit area.

The fill factor FF, the short-circuit current I_{SC} and the open-circuit voltage V_{OC} are independently computed to obtain the maximum power P_{MPP}. In the rest of this study, it is assumed that the operating point is the maximum power point (MPP). Note that this work only models the direct current (DC) side of PV power. To have a complete estimation for a real PV system, further considerations would be necessary, like the eventual mismatch between modules in the same string, possible losses from the inverter MPP tracker strategies and the inverter efficiency that typically depends on the input DC power, among other factors.

As $R_{sh} = \infty$, I_{SC} equals the photogenerated current I_L. Hence it is directly related to the amount of solar energy converted into electric current, which depends on the spectral irradiance impinging on the module $G(\lambda)$, the spectral response of the material $SR(\lambda)$ and the cell temperature T_c:

$$I_{SC} = \left[\int_{\lambda} SR(\lambda)G(\lambda)d\lambda\right]\cdot(1 + C_{T,I_{SC}}\cdot(T_c - T_{c,STC})) \quad (3)$$

[2] freely available for research from https://confluence.ecmwf.int/display/ECRAD/ECMWF+Radiation+Scheme+Home.

Table 1
Wavenumber and wavelength limits of the 14 SW bands in ecRad.

Wavenumber cm^{-1}		Wavelength μm	
Minimum	Maximum	Minimum	Maximum
820	2600	3.84	12.2
2600	3250	3.07	3.84
3250	4000	2.50	3.07
4000	4650	2.15	2.50
4650	5150	1.94	2.15
5150	6450	1.55	1.94
6450	7700	1.29	1.55
7700	8050	1.24	1.29
8050	12850	0.778	1.24
12850	16000	0.625	0.778
16000	22650	0.442	0.625
22650	29000	0.345	0.442
29000	38000	0.263	0.345
38000	50000	0.200	0.263

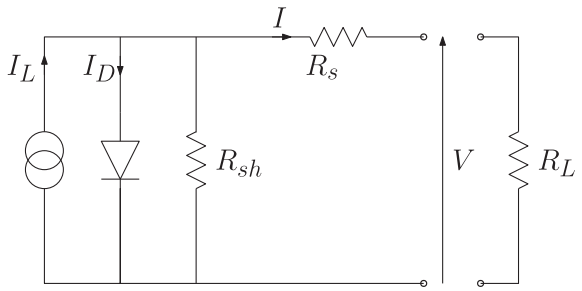

Fig. 4. Equivalent electrical circuit of a solar cell, with I_D the photodiode current, I_L the photogenerated current, and R_L and V the load resistance and voltage.

with $C_{T,I_{SC}}$ the short-circuit current temperature coefficient provided by the manufacturer accounting linearly for temperature effects.[3] Such a formulation accounts for the spectral and temperature effects but requires a fine spectral resolution irradiance at the cell-level, as well as an accurate estimation of the spectral response and the cell temperature. The other parameters ($C_{T,I_{SC}}$, $T_{c,STC}$) are provided by the manufacturer. With these notations, the APE (e.g. Norton et al., 2015) is defined as:

$$\mathrm{APE}(\lambda) = \frac{\int_\lambda G(\lambda)\mathrm{d}\lambda}{\int_\lambda \mathrm{SR}_{\mathrm{ideal}}(\lambda)G(\lambda)\mathrm{d}\lambda}. \tag{4}$$

V_{OC} is modelled as (Da Rosa, 2005; Messenger and Abtahi, 2017):

$$V_{OC} = V_t \ln\left(\frac{I_{SC}}{I_0}\right). \tag{5}$$

It mainly depends on T_c through the thermal voltage $V_t = kT_c/q$ term (with k the Boltzmann constant) and I_0 the reverse saturation current which is highly sensitive to temperature and computed following (Singh and Ravindra, 2012):

$$I_0(T_c) = CT_c^3 \cdot \exp\left(-\frac{E_g}{kT_c}\right). \tag{6}$$

The constant C is deduced from the manufacturer datasheet.[4] The temperature dependency of the energy gap E_g is neglected, according to Singh and Ravindra (2012).

FF is computed following Eq. (7) of Green (1982) and depends on I_{SC}, V_{OC}, V_t and R_s. R_s is assumed constant, and is computed by inverting the formulation of Green (1982) based on the STC characteristics.

To summarize, the PV model requires the cell temperature T_c, the spectral response $\mathrm{SR}(\lambda)$ and the cell impacting spectral irradiance $G(\lambda)$. The following details how these variables are computed from variables commonly output by atmospheric models, namely direct and diffuse horizontal incident irradiances, air temperature and wind speed. Fig. 5 illustrates the architecture of the PV model.

3.3.2. Cell temperature and spectral response

3.3.2.1. Cell temperature. T_c is modelled after King et al. (2004). First, the module temperature T_{mod} is computed from the air temperature T_a, the POA irradiance G_{POA} and U_{10m} the wind speed at 10 m (King et al., 2004):

$$T_{mod} = G_{POA}\exp(a + b \times U_{10m}) + T_a, \tag{7}$$

where $a = -3.23$ and $b = -0.13$ s m^{-1} were chosen from the parameters provided in King et al. (2004) because they resulted in the best match with measured module temperatures. T_c is then derived from T_{mod}:

$$T_c = T_{mod} + \frac{G_{POA}}{G_{ref}} \times \Delta T \tag{8}$$

where $\Delta T = 13$K for $G_{ref} = 1000$ Wm^{-2} is also taken from King et al. (2004).

3.3.2.2. Spectral response. Contrary to the ideal SR introduced in Section 2.1, the actual SR is specific to each individual module because a reduced response can be caused by module-specific factors like surface recombination, non-optimal absorption or ageing. Unless the SR is provided by the user, a systematic approach based on the ideal formulation is used. It consists in scaling the ideal spectral response by a factor α:

$$\mathrm{SR}_{\mathrm{modelled}}(\lambda) = \alpha \times \mathrm{SR}_{\mathrm{ideal}}(\lambda). \tag{9}$$

α is set such that the current is correctly computed in STC. It is computed as:

$$\alpha = \frac{I_{SC,STC}}{\int_\lambda \mathrm{SR}_{\mathrm{ideal}}(\lambda)G_{c,\mathrm{ASTM}}(\lambda)\mathrm{d}\lambda}, \tag{10}$$

with $G_{c,ASTM}$ the cell-impacting irradiance resulting from an incoming ASTM reference spectrum in the POA, accounting for optical losses. Here $\alpha = 0.77$. The constant α remains however dependent on the module considered, as the ideal spectral response relies on λ_{gap}, which is technology-specific. Note that taking a more realistic spectral response may alter the following results, as discussed in Section 4.2.

3.3.3. Cell impacting spectral irradiance

Whereas the previous components of the PV code were essentially built from the literature, the novelty of the code is the subsequent treatment of spectral irradiance, which allows to get $G(\lambda)$ at high spectral resolution whatever the resolution of the irradiance input. It is assumed that the direct and diffuse horizontal irradiances are provided in a limited number of spectral bands. If only the GHI is provided, a preliminary step should be used to decompose GHI into direct and diffuse irradiance. The cell impacting spectral irradiance is modelled by first computing the POA irradiance from the direct and diffuse components (transposition step detailed below), then by applying optical losses which account for reflection at the surface of the module. The cell impacting irradiance, later convolved by the SR, should have a spectral resolution fine enough to account for the spectral dependence of the SR and in particular its sharp discontinuity around λ_{gap}. To this end, the low resolution direct and diffuse horizontal irradiances are first manipulated to reach the resolution of the reference ARTDECO spectra.

[3] The STC subscript refers to the Standard Test Conditions (Sun-facing module with an inclination of , incident irradiance of 1000 Wm^{-2} with the solar spectrum for an air mass of 1.5, cell temperature $T_{c,STC} = 25$ °C).

[4] One can easily deduce from Eq. 5 and Eq. 6 that $C = I_{SC,STC}(T_{c,STC})^{-3}\exp\left(\frac{\frac{E_g}{q} - V_{OC,STC}}{V_t(T_{c,STC})}\right)$.

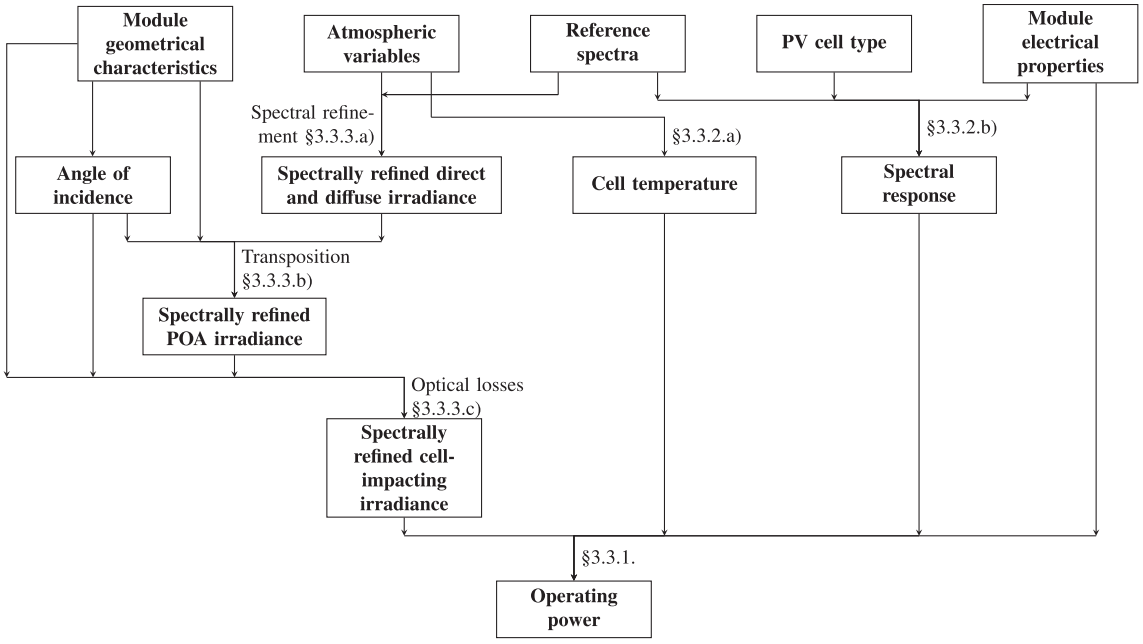

Fig. 5. Simplified workflow of the PV model.

The procedure is detailed below.

3.3.3.1. Refining the spectral resolution. The refinement of spectral resolution aims at detailing the relative distribution of energy within each spectral band of the input irradiances. This is achieved by applying the resolution and shape of a reference spectrum G_{ref} to the narrow-band spectrum whilst conserving the total amount of energy within each band. The fine resolution irradiance for $\lambda \in [\lambda_k;\lambda_{k+1}]$ (where λ_k and λ_{k+1} are the lower and upper boundaries of band k) is computed as follows:

$$G(\lambda) = G_k \frac{G_{\text{ref}}(\lambda)}{\int_{\lambda_k}^{\lambda_{k+1}} G_{\text{ref}}(\lambda)\mathrm{d}\lambda}, \tag{11}$$

where G_k is the irradiance in band k. This method leads to discontinuities at each band limit but allows to better account for the actual distribution within a band. Note that commonly used quantities such as APE, MM and UF can all be computed from $G(\lambda)$.

The choice of the reference spectrum is key to accurately inform about the spectral distribution of irradiance. Given that direct and diffuse irradiances have very distinct spectral distributions, both components are spectrally refined separately using direct and diffuse reference spectra. The spectral distribution also depends on SZA and atmospheric conditions (Liou, 2002). To account for this, a collection of clear-sky reference spectra is considered, with SZA ranging from 5° to 85° by steps of 5°. All reference spectra are computed with the same atmospheric characteristics (water vapour, ozone, aerosols). Extending the set of reference spectra to other variables would substantially increase the complexity of the model. Furthermore, the exact atmospheric conditions are already properly accounted for in the total energy per band provided by the irradiance inputs, which is conserved when refining the resolution. Only changes in spectral shape within a band might be missed with this limited set of reference spectra, but this is secondary with regards to the general shape of a solar spectrum. In other terms, limiting the reference spectra to only various SZAs enables us to keep the model simple whilst explaining most features of the spectral distribution.

Fig. 6 illustrates the steps required for refining the spectral resolution of direct surface irradiance obtained from ecRad in the case of an optically thin cloud ($\tau = 2.3$). The reference spectrum is computed by interpolation of the direct ARTDECO spectra for the given SZA (Fig. 6b). The initial irradiance (Fig. 6a) is then spectrally refined following Eq. 11 which leads to a spectrum of the same resolution as the reference spectrum (Fig. 6b).

3.3.3.2. Transposition. Transposition of the direct component on the POA simply depends on SZA, SAA (Solar Azimuth Angle), and the

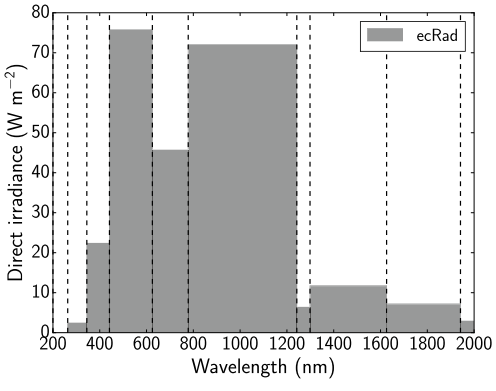

(a)

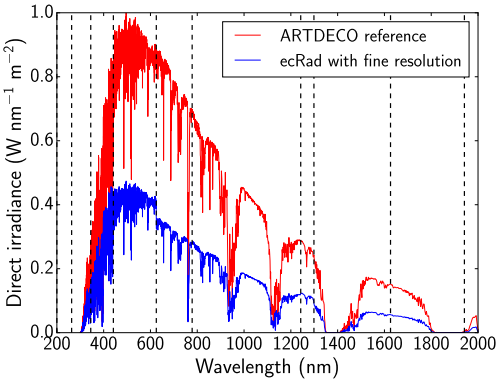

(b)

Fig. 6. Illustration of the spectral refinement step used in the PV model. (a) Low-resolution direct irradiance computed by ecRad for a thin cloud with optical thickness 2.3. (b) Corresponding ARTDECO clear-sky direct irradiance at the same SZA, and spectrally refined ecRad irradiance using the reference spectrum. The dotted lines indicate ecRad bands.

module inclination and azimuth (Duffie and Beckman, 2013). For the diffuse component, a hypothesis on the angular distribution over the sky dome is required to account for the equivalent angle-of-incidence on the module. A variety of transposition models are available in the literature. Here, it is chosen based on a thorough comparison of broadband POA irradiances measured at the SIRTA on the one hand, and computed from direct and diffuse broadband horizontal irradiances on the other hand. Practically, it follows the approach from Badescu (2002) for SZA < 70° and Perez et al. (1990) otherwise. The ground-reflected component follows the approach from Badescu (2002) except for SZA > 70° where the 2D isotropic model (e.g. Duffie and Beckman, 2013) is applied. Although these choices were constrained by very specific observations, they are sufficiently physically relevant to meet our objectives. Note also that these parameterisations were initially developed for broadband quantities but are extended here to spectrally-refined irradiances.

3.3.3.3. Optical losses. Optical losses result from reflection at the panel surface. Although they are wavelength-dependent, Sjerps-Koomen et al. (1996) show that this dependence can be neglected. They also conclude that optical losses mostly result from the air-glass interface. For this reason, the optical losses OL applied here correspond to the proportion of incident radiation that is reflected at the air-glass interface (Sjerps-Koomen et al., 1996):

$$\mathrm{OL} = \frac{1}{2}\left(\frac{\sin^2(\theta_i - \theta_r)}{\sin^2(\theta_i + \theta_r)} + \frac{\tan^2(\theta_i - \theta_r)}{\tan^2(\theta_i + \theta_r)}\right), \tag{12}$$

with θ_i and θ_r the angles of incidence and refraction at the air-glass interface. θ_i is computed from the SZA, SAA and module orientation and θ_r is computed after Snell's law:

$$\theta_r = \arcsin\left(\frac{n_0}{n_1}\sin(\theta_i)\right), \tag{13}$$

with $n_0 = 1$ and $n_1 = 1.526$ the refractive indexes of air and glass (De Soto et al., 2006). Note that this approach does not consider any antireflective coating. Adding such a layer would imply adding module specific parameters not informed by the manufacturer datasheet. Furthermore, this simple model already corrected most errors in PV power at low SZA when validating against measurements at SIRTA. Given the difference in effective angle-of-incidence for direct, diffuse and reflected contributions to POA irradiance, the optical losses are computed independently for all three components. The effective incident angle for diffuse and reflected components are computed following (Brandemuehl and Beckman, 1980).

3.4. Code validation

The PV model has been validated against SIRTA measurements spanning January 2015 – June 2017. The measured broadband global and diffuse irradiances, wind speed and air temperature are used as inputs to the PV model. The spectral surface albedo is that of vegetation to be consistent with SIRTA environment. Over the whole period, when SZA<80°, the simulated PV power for the 250 W panel has a mean relative error (MRE[5]) of −0.9%, a mean bias of − 2.0 W and a root mean squared error of 13.2 W compared to observations. The MRE is chosen instead of the mean error to stress that the model behaves well even at grazing solar angles.

The measured PV power has been regressed against the simulated POA irradiance (correlation coefficient $r = 0.970$), the simulated POA irradiance corrected for temperature[6] ($r = 0.972$) and the simulated PV power ($r = 0.977$). Although the differences are small, the correlation coefficients suggest that simulated PV power is more informative than simulated POA. They also suggest that using a detailed PV model to treat the spectral effects is as crucial as accounting properly for the temperature effect on P_{MPP}. This added value would certainly be more significant if the inputs to the PV model were not broadband, but instead featured several spectral bands to better constrain the spectral distribution of incident irradiance.

The PV model performs well under clear skies with no systematic bias. Fig. 7 shows the measured and simulated PV power over a period of seven consecutive cloudy days. In overcast conditions the PV model tends to underestimate the power. This probably stems from the fact that reference spectra are clear-sky, meaning that the actual useful fraction of irradiance is underestimated. The choice of the transposition model for diffuse radiation and the complex irradiance fields due to scattered clouds can also contribute to the observed differences.

Although informative, this evaluation does not fully bring out the potential and novelty of this code, as the inputs are broadband. Furthermore, the errors can be due to the distance between the irradiance measurements fed into the PV code and the effective position of the PV modules (~700 m). Also, the model has only been validated for one site, and would deserve to be validated at other locations, in particular with other cloud regimes. Last, the PV model does not require any measurements of the POA irradiance or PV power and fully relies on the datasheet provided by the manufacturer, which has not been rigorously verified. As a consequence, any deviation from the specifications is detrimental to the PV model. The focus of this paper is not on the absolute performance of this model, though. The model was more designed as a physically comprehensive tool to study the influence of spectral and angular details of surface solar irradiance on PV performance through the impact of clouds.

3.5. Sensitivity of simulated PV power to atmospheric inputs

In the rest of this study, a c-Si module is considered with an inclination of 27° (identical to the one used for the code validation) to mimic the setup at SIRTA. The influence of clouds on PV performance estimation is studied by providing ecRad spectra to the PV model. ecRad simulations are performed for various SZA and optical thicknesses of the 1 km-thick cloud. The 14-band direct and diffuse horizontal irradiances outputs are input to the PV model to simulate the PV power. The cell temperature is set constant to STC temperature, such that irradiance is the only variable affecting PV power. In the following, two performance definitions are discussed: the standard performance ρ defined as the ratio of PV power to broadband POA irradiance and the in-band performance ρ^*. The latter only considers the useful POA irradiance (i.e. up to λ_{gap}).

The impact of spectral and angular details on the modelled PV power is studied based on the same ecRad inputs. The 14-band direct and diffuse horizontal irradiances (Fig. 8a) are postprocessed to constitute three declined levels of information: they are first integrated over every 2 consecutive bands resulting in a 7-band input (Fig. 8b) and and then over all bands leading to a 1-band input (Fig. 8c) for the PV model. A further degradation is considered by summing the direct and diffuse components of the 1-band irradiance (Fig. 8d). In this case, the decomposition between direct and diffuse irradiance follows (Erbs et al., 1982).

4. Results

4.1. Spectral and angular effect of clouds on PV performance

4.1.1. Impact of cloud optical thickness

Fig. 9a indicates that the in-band performance ρ^* decreases with optical thickness for all simulated SZAs. It drops from 19.3% to 15.8% for τ ranging from 0 to 50 when SZA = 70°. This can be explained by

[5] $\mathrm{MRE} = \frac{1}{N}\sum_{i=1}^{N}\frac{P^i_{\mathrm{sim}} - P^i_{\mathrm{MPP}}}{P^i_{\mathrm{MPP}}}$.

[6] that is POA irradiance multiplied by $(1 - C_{T,P_{\mathrm{MPP}}}(T - T_{c,\mathrm{STC}}))$ to include the effect of temperature on P_{MPP} provided by the manufacturer.

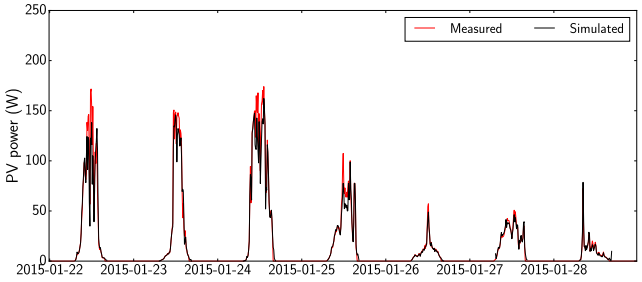

Fig. 7. Measured and simulated PV power at SIRTA over a period of seven cloudy days.

the spectral filtering of clouds that shifts the irradiance within the range [0 - λ_{gap}] towards the blue domain as the optical thickness increases, combined with a reduced SR in this domain.

The opposite behaviour is generally observed for SZA < 50° – domain over which most PV energy is harvested – when the total POA irradiance is considered (Fig. 9b). Up to a critical optical thickness τ_{crit}(SZA), clouds enhance the PV performance ρ, with gains up to 5.7% (for SZA = 0°). The difference between ρ and ρ^* is interpreted as follows: due to the spectral filtering of clouds, photons that are not energetic enough to be absorbed by the PV module are filtered out by the clouds. The useful fraction (UF) of irradiance (hence ρ) thus increases with τ, as illustrated for instance in Fig. 10. Likewise, the APE increases

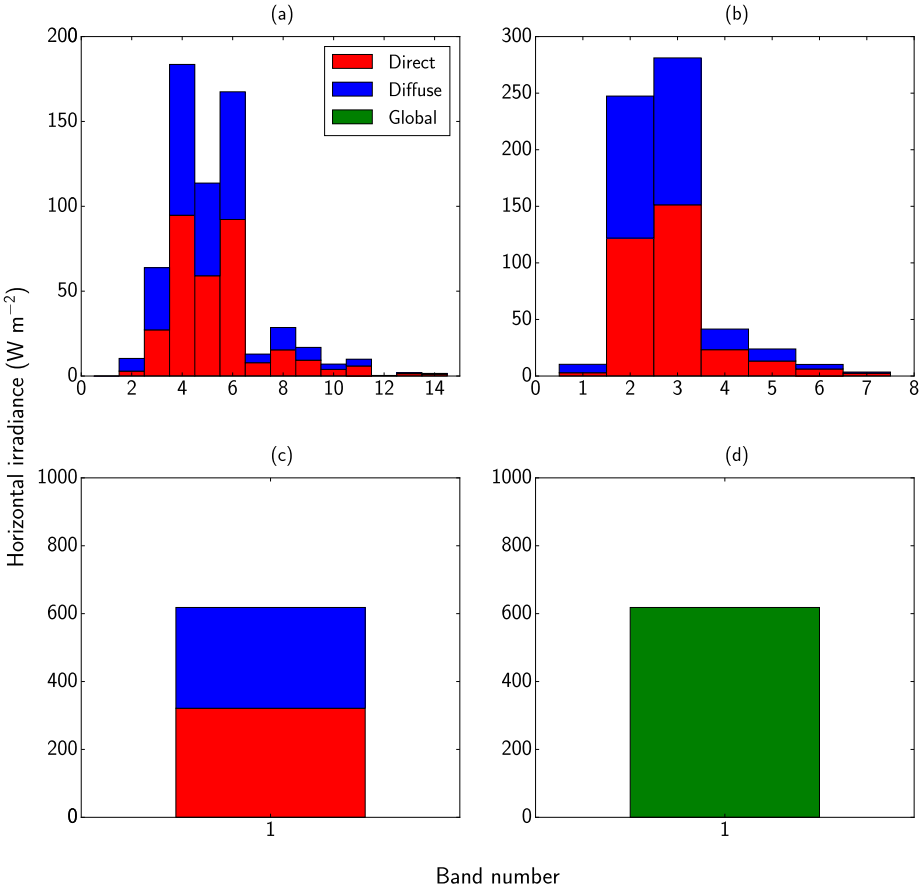

Fig. 8. Illustration of the 4 input configurations obtained from ecRad simulations: 14 (a), 7 (b) and 1 (c) spectral bands, as well as solely GHI (d). The simulation corresponds to a cloudy atmosphere (τ = 1.73) with SZA = 48°.

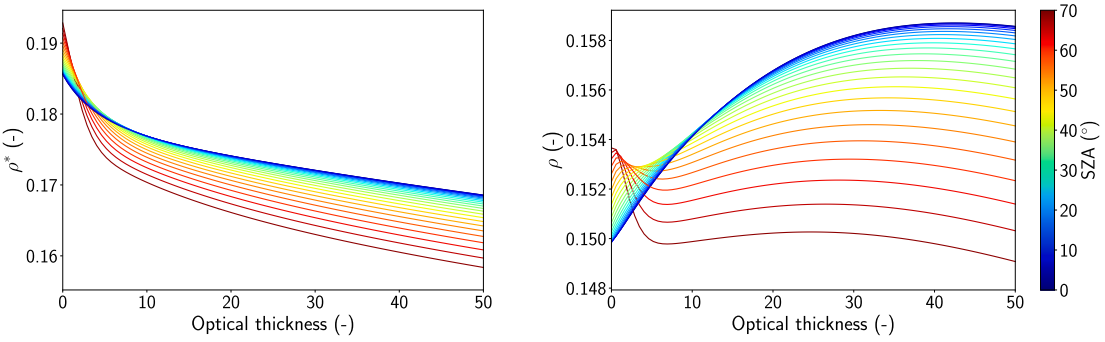

(a) POA irradiance in silicon cell sensitive domain

(b) Total POA irradiance

Fig. 9. Simulated performance of the c-Si module as a function of cloud optical thickness and SZA.

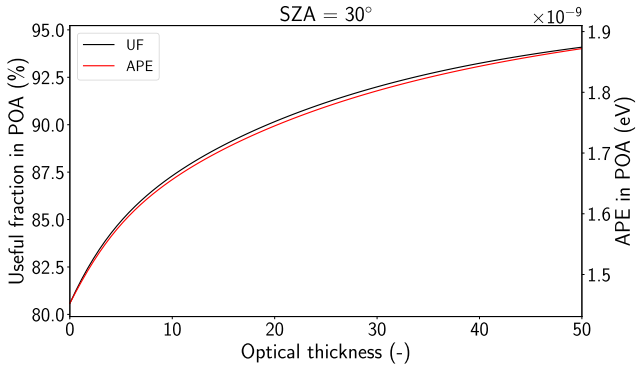

Fig. 10. Variations of the useful fraction ($\lambda < 1100$ nm) and average photon energy (over the whole spectrum) of POA irradiance with optical thickness for SZA = 30°.

as the incident spectrum becomes richer in shorter and more energetic wavelengths. For high optical thicknesses (above $\tau_{crit}(SZA)$), ρ starts to decrease. At such optical thicknesses, wavelengths larger than λ_{gap} have been widely filtered out such that POA irradiance approaches useful POA irradiance, and ρ behaves more like ρ^*. A distinct behaviour is observed for large SZAs. In such case, the cloud effect is enhanced and direct radiation rapidly vanishes due to its long path through the cloud. The part of the spectrum where the spectral response is maximum is thus quickly filtered out and ρ behaves as ρ^*. The conversion from ρ^* to ρ is equivalent to multiplying ρ^* by UF, which increases with τ (Fig. 10), hence explaining the complex variations observed in Fig. 9b, in particular for $\tau < 5$.

4.1.2. Impact of the solar zenith angle

Fig. 9b shows that under clear-sky conditions ρ increases with SZA, whilst the opposite prevails in cloudy conditions. In addition, at SZA larger than ~50°, ρ does not increase monotonically with τ. In clear-sky conditions, direct radiation is the main contributor to the POA irradiance, and its contribution grows with SZA as it becomes more and more normal to the module (Fig. 11b). For larger SZA, the contribution of direct radiation decreases because it becomes less perpendicular to the panel and because diffuse radiation increases with SZA. However, ρ further increases because at the same time, the performance of the module increases due to the spectral changes of irradiance. Note that this balance between relative contribution of direct radiation and spectral effects depends on the inclination angle of the panel, so that slightly different dependences on SZA may be encountered at different β. On the contrary, for optically thick clouds, the POA irradiance is essentially diffuse and results from the mixing of direct and diffuse radiation impacting the cloud top. The relative preponderance of blue light at cloud top increases with SZA, which explains why the performance decreases with SZA. In other words, SZA has under clear skies a geometric effect through the relative contribution of the more efficient direct irradiance, whereas under cloudy skies, SZA has a spectral effect on PV performance similar to that of optical thickness due to the wavelength-selective Rayleigh scattering.

To conclude, the impact of clouds on radiation can be explained by two levels of spectral filtering. First, clouds tend to increase the performance of a PV module as they filter out photons with insufficient energy. Second, due to the shift from NIR towards the blue domain, the effect is opposite when only the useful irradiance is considered. SZA also affects the performance, by controlling the contribution of direct radiation and the path length through the atmosphere. This overall stresses that there is no simple relationship between POA irradiance and PV power.

4.2. Spectral resolution

The previous section used 14-band irradiance inputs. Yet, irradiance obtained from measurements or atmospheric models is often integrated over the whole SW domain or a limited number of bands. The following section investigates the impact of this limited information on simulated power. PV power is simulated for all {SZA, τ} combinations used in Section 4.1, and the three degraded inputs introduced in Section 3.5. Fig. 12 shows the relative difference between the power simulated with the degraded inputs and the reference 14-band input.

The 7-band configuration is more precise (up to −3% error) than the 1-band (up to −10% error). Generally, errors increase with optical thickness, as spectral effects gain in importance. As the number of bands declines, spectral filtering by clouds is less captured and cannot be correctly accounted for by the spectral refinement. The difference between the 7- and 14-band configurations suggests that a dozen bands should practically be enough to achieve satisfactory performance. Also, the reference ARTDECO spectra used for spectral refinement have been computed under clear-sky conditions. Hence, when only one band is provided, the highly resolved irradiance corresponds to a clear-sky spectrum, thus leading to underestimated power, which explains the negative errors. The sensitivity to SZA remains limited thanks to the use of SZA-interpolated ARTDECO reference spectra. When only the GHI is known, the relative errors range from −10% to 10% and present no general trend over SZA or τ. This largest range of relative errors and the non-monotonous variability with atmospheric conditions point out that the GHI is not a sufficient input parameter for PV modelling. Despite this deficiency, it probably remains the most extensively used quantity to feed PV models.

Although Fig. 12 was obtained with an ideal spectral response, it was also computed (not shown) assuming a more realistic spectral response for the c-Si module (from https://pvpmc.sandia.gov/modeling-steps/2-dc-module-iv/effective-irradiance/spectral-response/). The obtained patterns are very similar, but the relative errors are approximately 50% larger, highlighting that the spectral effect might be even

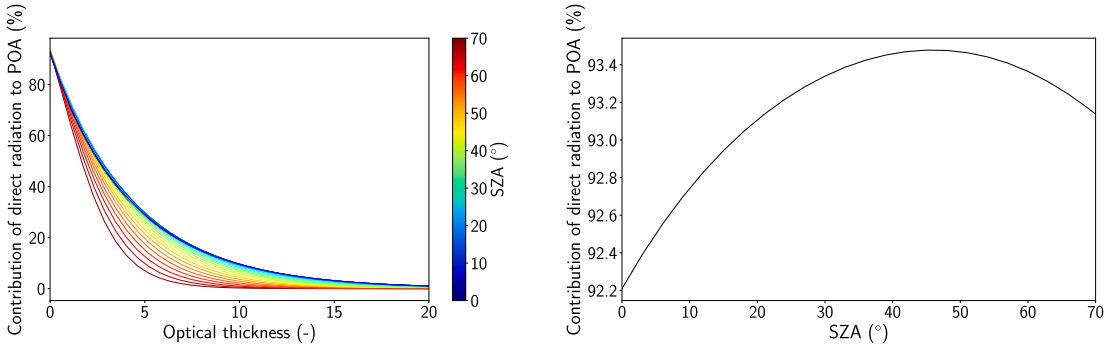

(a) For varying τ (b) For $\tau = 0$

Fig. 11. Contribution of the beam radiation to the total POA irradiance.

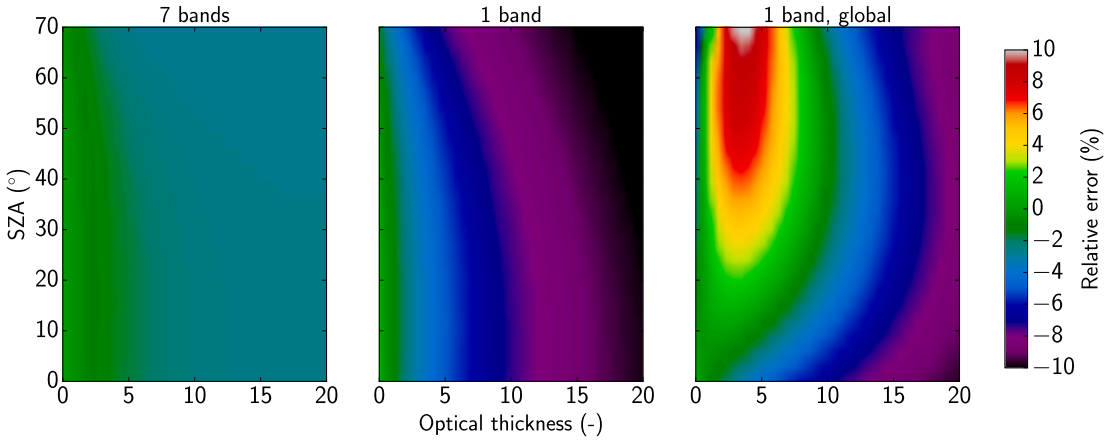

Fig. 12. Relative error in simulated PV power as a function of τ and SZA and for the 7-band, 1-band and 1-band global inputs, with respect to the 14-band input.

more significant with a realistic spectral response. Likewise, all the results presented above have been obtained without aerosols. Quantitative results may slightly change in the presence of aerosols but the overall trends and general conclusions would remain the same.

5. Discussion

5.1. Comparison to observations

5.1.1. Previous experimental studies

In the case of c-Si cells under clear skies, Stark and Theristis (2015) found that increasing SZAs causes spectral gains up to SZA $\approx 75-80°$ and losses beyond. Our results for SZA<70° support these results. Likewise the observations reported by Nofuentes et al. (2014) confirm the positive effect of clouds on ρ. The variations of ± 5% they noticed compared to STC are slightly larger than those obtained in this paper. Yet, their results are based on observations, meaning that other atmospheric variables may amplify the spectral effects. Last, Jardine et al. (2001) conclude that c-Si cells work more efficiently under clear skies based on a measurement campaign and an estimation of the cloud cover. However, Jardine et al. (2001) lack details on how PV efficiency is computed and their approach based on the cloud cover K_t instead of the cloud optical thickness does not enable a clear comparison between their results and this study.

5.1.2. In situ observations at SIRTA

Here an attempt is made to compare the PV performance obtained in the numerical simulations to observations made at SIRTA. To this end, the measured performance ρ is compared to that simulated in Fig. 9b. A SZA of 30° is chosen because it corresponds to summer conditions at noon at SIRTA and because Fig. 9b suggests that ρ is more sensitive to τ at low SZA. To be consistent with the simulations, the measured power is first corrected to the equivalent power at 25 °C ($T_{c,STC}$). Then, one performance value per day satisfying the following conditions is retained: (i) only measurements taken between 11h50 and 12h10 and such that SZA is between 27 and 33 ° are used and averaged in order to be comparable with the theoretical results obtained for SZA = 30°; (ii) at least two such measurements are available; (iii) the difference between the maximum and minimum incident SW radiation measurements is less than 0.3 times the average value to ensure relative stability of the cloud cover. The optical thickness τ of *in situ* clouds was estimated from the measured atmospheric transmittance, following Eq. (9) of Barnard and Long (2004).[7] Fig. 13 shows the measured and simulated performances as a function of cloud optical thickness. It indicates that the observations globally agree with the simulations in terms of absolute values (relative differences less than 7%). Significant deviations nevertheless remain and the dependence of ρ on τ is not obvious in the observations, making this comparison somehow inconclusive. This is not completely surprising because the simulations consider a fixed atmosphere with horizontally uniform cloud properties, whereas observations correspond to varying atmospheric conditions where physical quantities such as cloud geometry, cloud fraction, humidity and aerosol optical depth affect the spectral and angular properties of the irradiance, probably competing with clouds. Also, the optical thickness of a heterogeneous cloud is hard to define, which is further biased by the distance between the instruments related to irradiance and the PV modules. This suggests that assessing the impact of clouds on PV performance based on measurements is challenging because the uncertainty of measurements is similar in magnitude to the expected impact of clouds. Although a more quantitative identification of the sources of error for PV performance simulations would definitely be useful to improve PV models, this would require a more extensive set of measurements and a more thorough data analysis than intended in this study.

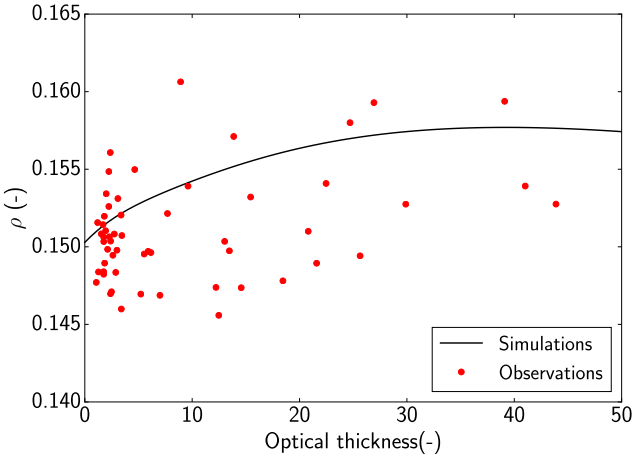

Fig. 13. Measured and simulated performances as a function of cloud optical thickness for SZA = 30 ± 3° and Sun-facing PV module. The measured performance is corrected to represent the equivalent performance at $T_{c,STC}$.

5.2. Application to NWP outputs

The present study is intentionally academic and does not pretend to quantify the global impact of using refined NWP outputs for PV power

[7] $\tau = \exp(2.15 + \alpha_s + 1.91 \operatorname{arctanh}(1 - 1.74r))$, where the surface albedo $\alpha_s = 0.2$ and $r = \frac{\mathrm{GHI}}{\mathrm{GHI_{cs}}\mu_0^{1/4}}$. $\mathrm{GHI_{cs}}$ is the theoretical GHI in clear sky conditions computed with ARTDECO, and $\mu_0 = \cos(\mathrm{SZA})$.

forecast or to demonstrate the quantitative benefit of using the developed PV model. Such an integrated investigation is is beyond the scope of the present paper. It would deserve a distinct dedicated work along with additional field observations. However, because the findings of Section 4.2 were obtained in very idealistic atmospheric conditions, this section aims at exploring more realistic and diverse atmospheric configurations. To this end, simulations are performed with the research atmospheric model Meso-NH (Lac et al., 2018) on a domain of 80 × 80 km centered on the SIRTA. Each simulation lasts 24 h and can be considered as a weather forecast. The following analysis focuses on June 2017. A month-long simulation enables to cover various atmospheric simulations as intended. June was chosen because it is when cumulated PV production is generally the largest. Atmospheric reanalysis from the AROME operational model (Seity et al., 2011) are used to initialize the Meso-NH simulations and to provide boundary conditions. The solar irradiance in Meso-NH is computed with ecRad, and the model was updated to output the direct and diffuse spectral irradiances in 14 spectral bands at the SIRTA. As in Section 4.2, these irradiances were post-processed to obtain various configurations which were fed into the PV model, allowing to compare the time series of PV power. Clouds in the simulations can be multi-layer and have physical properties varying with altitude, including effective radius which is diagnosed after Eq. (24)[8] of Martin et al. (1994), thus covering a variety of cloud conditions. In addition, aerosols optical depths are prescribed in Meso-NH based on climatological values.

The mean relative error in simulated PV power over June 2017 is 0.36% with 7 bands, and 1.00% for 1 band. When only GHI is used, the production is underestimated by only 0.30% but this is the result of error compensation at different SZA. The mean absolute relative error for this configuration is actually 2.78%. Because spectral effects are known to depend on PV technology, similar computations were performed for a CdTe panel which is more wavelength-selective (λ_{gap} = 806 nm). This resulted in larger mean relative errors of −0.5, 2.1 and 5.0% for the three configurations detailed above.

Fig. 14 shows the relative difference of simulated PV power between the degraded configurations and the reference 14-band configuration. The densest regions of points correspond to clear-sky conditions, which were prevailing in June 2017. In such conditions, the impact of degrading resolution is very marginal for the 7 bands and 1 band configurations, but it becomes significant for the 1 band global configuration as SZA increases, that is when the reference power decreases. The impact of clouds is in most cases to reduce the estimated PV power. This underestimation is around 2% for the 7 band configuration, but it often exceeds 10% for the 1 band configurations and reaches 20% for the 1 band global configuration. These results are consistent with those shown in Fig. 12, but encompass much more realistic cloudy conditions than those investigated in Section 4.2.

The Meso-NH simulations confirm that in cloudy conditions a poor representation of the spectral distribution of solar irradiance can result in large errors of PV power and consequently highlight the need for detailed irradiance inputs in cloudy conditions, which is the primary objective of the study. The monetary impact of the identified errors is very hard to estimate. It would require large scale NWP simulations over long periods, and a proper treatment of the penalties resulting from unbalance between day-ahead energy forecast and actual production (Antonanzas et al., 2017). Likewise, the impact on the management of the electricity grid will be very location-dependent and cannot be assessed based on this work. The operational impact of the present findings and the complementary analysis needed to tackle the pointed issues are thus left to experts.

[8] with N_{tot} = 900 cm^{-3} and d = 0.43.

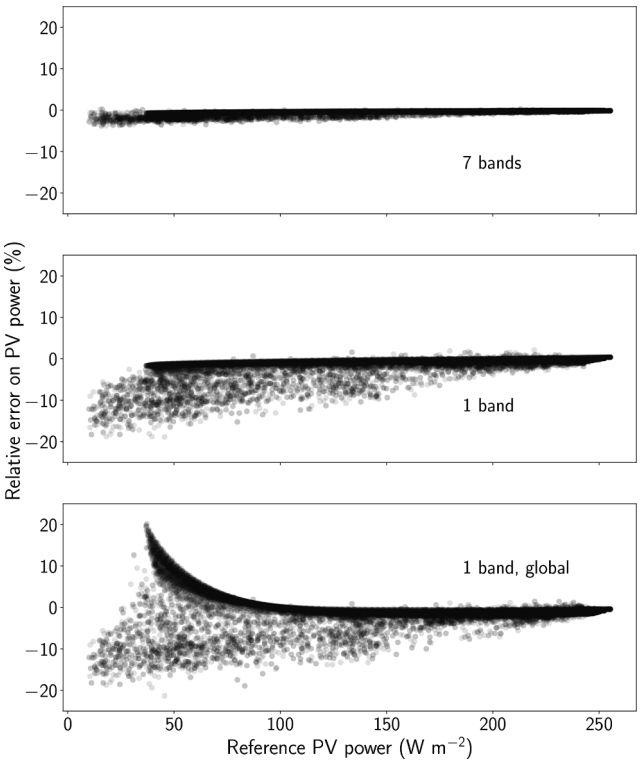

Fig. 14. Relative difference in PV power for various configurations of solar irradiance inputs with respect to the reference 14-band configuration, as a function of the reference power. The reference solar irradiance corresponds to 1-min-resolution Meso-NH simulations at SIRTA for June 2017. Other configurations are obtained via degradation of the reference configuration. Only simulations for SZA <70° and PV_{ref}> 10 W m^{-2} are used.

5.3. Practical impacts

This study shows that clouds alter PV power not only because they reduce the available POA irradiance, but also because they alter the performance of PV cells through spectral filtering. This is critical for studies using climate models to investigate the effect of climate change on PV performance or to compute PV potential atlases.

Our results clearly indicate that a given POA irradiance can result in different PV power because the relationship depends on atmospheric conditions. More importantly, GHI is shown to be far from sufficient to accurately model PV power as it lacks both angular and spectral information. Though most PV models make a hypothesis on the repartition between direct and diffuse radiation, only a few attempt to correct PV performance for the corresponding spectral changes. In both cases, GHI is used to deduce the direct and diffuse irradiances thanks to measured or simulated ancillary quantities, which means that PV models attempt to reconstruct atmospheric conditions. The aim of the newly developed PV model is to overcome this loss of information between the atmospheric model and the PV model by directly exploiting the internal variables of atmospheric models. As such it is expected to reduce the overall computation time by limiting the number of extra steps. Hence the apparent complexity of the physical model should not be a critical obstacle to its utilization, unless it is proven definitely too complex for specific applications.

The present work focused on c-Si cells, which are less sensitive to spectral effects than other solar cells with a smaller λ_{gap} (Nofuentes et al., 2014; Dirnberger et al., 2015) such as CdTe and a-Si cells, as illustrated in Section 5.2. The impact of clouds on PV performance are time, location and technology dependent, so that a more quantitative analysis would require a dedicated study that is beyond the scope of the present paper. For instance, the impacts are expected to be more

significant in cloudy areas, while they may be insignificant in sunny areas. However, accounting for spectral effects would be all the more relevant for such sensitive technologies and could be the focus of future studies.

6. Conclusion

This study investigated the benefit of using angularly and spectrally detailed irradiance inputs in PV models that convert atmospheric variables into PV power. Such a model has been developed with the intent to fully take advantage of the internal spectral radiative quantities of atmospheric models or radiative transfer codes. It properly accounts for the spectral and angular impacts of incident radiation on PV performance, in particular through the spectral resolution refinement of the irradiance inputs which is essential to cope with the low spectral resolution of atmospheric models outputs and to match the sharp spectral response of PV cells. Based on this model, the sensitivity of simulated PV power to the resolution of the irradiance inputs has been explored. This work indicates that the presence of clouds, through spectral filtering, can increase PV performance by more than 5%, and that similar variations are expected when varying the solar zenith angle (SZA). The model was also used to assess the errors committed when incident irradiance input to the PV model is only poorly known, that is when it lacks spectral or angular information. It was shown that using a single spectral band results in errors up to 10%, which amount to 15% when solely the Global Horizontal Irradiance (GHI) is fed into the PV model. It also suggests that a dozen spectral bands should be sufficient to correctly account for the spectral effects of clouds. These theoretical findings were supported by the analysis of spectral irradiances outputs of a NWP model corresponding to complex and more realistic atmospheric states. Although most PV models use standard atmospheric inputs which lack information, this study highlights that efforts should be made to fully take advantage of atmospheric models which generally deal with more informative internal variables, stressing the need for closer ties between the solar energy and atmospheric sciences communities. This is all the more relevant as this information could be gained without any increase in computation efficiency. Practically, these internal variables are not stored nowadays, simply because the extra storage space it would imply is not justified by well identified applications. The solar energy community could make it change by showing a strong interest for such quantities. Even though the highlighted spectral effects are much smaller than the errors in irradiance forecasts due to the inherent complexity of treating cloud heterogeneity and 3D radiative effects in NWP models, properly handling the currently available products can already substantially help to refine solar power prediction reliability. This project paves the way to further analyses related to the impact of spectral and angular properties of radiation on PV power. In particular, a similar study on aerosols shall be performed in the future, because alike clouds, different aerosols have different spectral and angular impacts on solar radiation, which cannot be quantified solely by their optical depth.

Declaration of Competing Interest

The authors declare that they have no known competing financial interests or personal relationships that could have appeared to influence the work reported in this paper.

Acknowledgements

This work was supported by the French national program LEFE/INSU through the CASPER project and the TREND-X research program of Ecole Polytechnique. The authors are grateful to Laurent Labonnote for helpful discussions on ARTDECO and to Christine Lac for the design of Meso-NH simulations.

References

Antonanzas, J., Osorio, N., Escobar, R., Urraca, R., Martinez-de Pison, F., Antonanzas-Torres, F., 2016. Review of photovoltaic power forecasting. Sol. Energy 136, 78–111.
Antonanzas, J., Pozo-Vázquez, D., Fernandez-Jimenez, L., Martinez-de Pison, F., 2017. The value of day-ahead forecasting for photovoltaics in the Spanish electricity market. Sol. Energy 158, 140–146.
Badescu, V., 2002. 3D isotropic approximation for solar diffuse irradiance on tilted surfaces. Renewable Energy 26 (2), 221–233.
Badosa, J., Bourdin, V., Haeffelin, M., Le, G., 2015. Multi-technology photovoltaic module test bench on the SIRTA meteorological and climate observatory. In: 31st European PV Solar Energy Conference and Exhibition.
Barnard, J.C., Long, C.N., 2004. A simple empirical equation to calculate cloud optical thickness using shortwave broadband measurements. J. Appl. Meteorol. 43 (7), 1057–1066.
Brandemuehl, M., Beckman, W., 1980. Transmission of diffuse radiation through CPC and flat plate collector glazings. Sol. Energy 24 (5), 511–513.
Da Rosa, A.V., 2005. Fundamentals of Renewable Energy Processes, first ed. Academic Press.
Das, U.K., Tey, K.S., Seyedmahmoudian, M., Mekhilef, S., Idris, M.Y.I., Van Deventer, W., Horan, B., Stojcevski, A., 2018. Forecasting of photovoltaic power generation and model optimization: A review. Renew. Sustain. Energy Rev. 81, 912–928.
De Soto, W., Klein, S., Beckman, W., 2006. Improvement and validation of a model for photovoltaic array performance. Sol. Energy 80 (1), 78–88.
Diagne, M., David, M., Lauret, P., Boland, J., Schmutz, N., 2013. Review of solar irradiance forecasting methods and a proposition for small-scale insular grids. Renew. Sustain. Energy Rev. 27, 65–76.
Dirnberger, D., Blackburn, G., Müller, B., Reise, C., 2015. On the impact of solar spectral irradiance on the yield of different PV technologies. Sol. Energy Mater. Sol. Cells 132, 431–442.
Duffie, J.A., Beckman, W.A., 2013. Solar Engineering of Thermal Processes. John Wiley & Sons.
Edwards, J., Slingo, A., 1996. Studies with a flexible new radiation code. I: choosing a configuration for a large-scale model. Quart. J. Roy. Meteorol. Soc. 122 (531), 689–719.
Erbs, D., Klein, S., Duffie, J., 1982. Estimation of the diffuse radiation fraction for hourly, daily and monthly-average global radiation. Sol. Energy 28 (4), 293–302.
Frouin, R., Ramon, D., Jolivet, D., Compiègne, M., 2018. Specifying algorithm uncertainties in satellite-derived PAR products. In: Remote Sensing of the Open and Coastal Ocean and Inland Waters. vol. 10778. International Society for Optics and Photonics, p. 107780W.
Ghitas, A.E., 2012. Studying the effect of spectral variations intensity of the incident solar radiation on the Si solar cells performance. NRIAG J. Astron. Geophys. 1 (2), 165–171.
Gottschalg, R., Betts, T., Williams, S., Sauter, D., Infield, D., Kearney, M., 2004. A critical appraisal of the factors affecting energy production from amorphous silicon photovoltaic arrays in a maritime climate. Sol. Energy 77 (6), 909–916.
Gottschalg, R., Infield, D., Kearney, M., 2003. Experimental study of variations of the solar spectrum of relevance to thin film solar cells. Sol. Energy Mater. Sol. Cells 79 (4), 527–537.
Green, M.A., 1982. Accuracy of analytical expressions for solar cell fill factors. Sol. Cells 7 (3), 337–340.
Gueymard, C.A., Ruiz-Arias, J.A., 2016. Extensive worldwide validation and climate sensitivity analysis of direct irradiance predictions from 1-min global irradiance. Sol. Energy 128, 1–30.
Haeffelin, M., Barthès, L., Bock, O., Boitel, C., Bony, S., Bouniol, D., Chepfer, H., Chiriaco, M., Cuesta, J., Delanoë, J., et al., 2005. SIRTA, a ground-based atmospheric observatory for cloud and aerosol research. Ann. Geophys. 23, 253–275.
Hale, G.M., Querry, M.R., 1973. Optical constants of water in the 200-nm to 200-μm wavelength region. Appl. Opt. 12 (3), 555–563.
Hess, M., Koepke, P., Schult, I., 1998. Optical properties of aerosols and clouds: the software package OPAC. Bull. Am. Meteorol. Soc. 79 (5), 831–844.
Hogan, R.J., Bozzo, A., 2018. A flexible and efficient radiation scheme for the ECMWF model. J. Adv. Model. Earth Syst.
Jardine, C.N., Conibeer, G.J., Lane, K., 2001. PV-COMPARE: direct comparison of eleven PV technologies at two locations in northern and southern Europe. In: Seventeenth EU PVSEC.
Jerez, S., Tobin, I., Vautard, R., Montávez, J.P., López-Romero, J.M., Thais, F., Bartok, B., Christensen, O.B., Colette, A., Déqué, M., et al., 2015. The impact of climate change on photovoltaic power generation in Europe. Nat. Commun. 6, 10014.
Jimenez, P.A., Hacker, J.P., Dudhia, J., Haupt, S.E., Ruiz-Arias, J.A., Gueymard, C.A., Thompson, G., Eidhammer, T., Deng, A., 2016. WRF-Solar: Description and clear-sky assessment of an augmented NWP model for solar power prediction. Bull. Am. Meteorol. Soc. 97 (7), 1249–1264.
Joseph, J.H., Wiscombe, W., Weinman, J., 1976. The delta-Eddington approximation for radiative flux transfer. J. Atmos. Sci. 33 (12), 2452–2459.
King, D.L., Boyson, W.E., Kratochvil, J.A., 2004. Photovoltaic array performance model. Tech. rep., Sandia National Laboratories.
King, D.L., Kratochvil, J.A., Boyson, W.E., 1997. Measuring solar spectral and angle-of-incidence effects on photovoltaic modules and solar irradiance sensors. In: Photovoltaic Specialists Conference, 1997, Conference Record of the Twenty-Sixth IEEE. IEEE, pp. 1113–1116.
Kirn, B., Topic, M., 2017. Diffuse and direct light solar spectra modeling in PV module performance rating. Sol. Energy 150, 310–316.
Kokhanovsky, A., 2004. Optical properties of terrestrial clouds. Earth Sci. Rev. 64 (3–4),

189–241.
Kostylev, V., Pavlovski, A.E.A., 2011. Solar power forecasting performance-towards industry standards. In: 1st International Workshop on the Integration of Solar Power into Power Systems, Aarhus, Denmark.
Lac, C., Chaboureau, P., Masson, V., Pinty, P., Tulet, P., Escobar, J., Leriche, M., Barthe, C., Aouizerats, B., Augros, C., et al., 2018. Overview of the Meso-NH model version 5.4 and its applications. Geosci. Model Develop. 11, 1929–1969.
Liou, K.-N., 2002. An Introduction to Atmospheric Radiation, vol. 84 Academic Press.
Lohou, F., Patton, E.G., 2014. Surface energy balance and buoyancy response to shallow cumulus shading. J. Atmosp. Sci. 71 (2), 665–682.
Lorenzo, E., 2003. Energy collected and delivered by PV modules. Handbook Photovolt. Sci. Eng. 905–970.
Marion, B., 2012. Influence of atmospheric variations on photovoltaic performance and modeling their effects for days with clear skies. In: 2012 38th IEEE Photovoltaic Specialists Conference. IEEE, pp. 003402–003407.
Martin, G., Johnson, D., Spice, A., 1994. The measurement and parameterization of effective radius of droplets in warm stratocumulus clouds. J. Atmos. Sci. 51 (13), 1823–1842.
Mayer, B., Kylling, A., 2005. The libRadtran software package for radiative transfer calculations-description and examples of use. Atmos. Chem. Phys. 5 (7), 1855–1877.
Messenger, R.A., Abtahi, A., 2017. Photovoltaic Systems Engineering. CRC Press.
Mittag, M., Vogt, L., Herzog, C., Pfreundt, A., Shahid, J., Neuhaus, D.H., Wirth, H., 2019. Thermal modelling of photovoltaic modules in operation and production. In: 36th European Photovoltaic Solar Energy Conference and Exhibition (EUPVSEC).
Mlawer, E.J., Taubman, S.J., Brown, P.D., Iacono, M.J., Clough, S.A., 1997. Radiative transfer for inhomogeneous atmospheres: RRTM, a validated correlated-k model for the longwave. J. Geophys. Res.: Atmos. 102 (D14), 16663–16682.
Morcrette, J., Barker, H., Cole, J., Iacono, M., Pincus, R., 2008. Impact of a new radiation package, McRad, in the ECMWF Integrated Forecasting System. Mon. Weather Rev. 136 (12), 4773–4798.
Myers, D., Emery, K., Gueymard, C., 2002. Proposed reference spectral irradiance standards to improve concentrating photovoltaic system design and performance evaluation. In: Photovoltaic Specialists Conference, 2002. Conference Record of the Twenty-Ninth IEEE. IEEE, pp. 923–926.
Myers, D.R., Gueymard, C.A., 2004. Description and availability of the SMARTS spectral model for photovoltaic applications. In: SPIE Proceedings Series. Society of Photo-Optical Instrumentation Engineers, pp. 56–67.
Nielsen, K.P., Gleeson, E., Rontu, L., 2014. Radiation sensitivity tests of the HARMONIE 37h1 NWP model. Geosci. Model Develop. 7 (4), 1433–1449.
Nofuentes, G., García-Domingo, B., Muñoz, J., Chenlo, F., 2014. Analysis of the dependence of the spectral factor of some PV technologies on the solar spectrum distribution. Appl. Energy 113, 302–309.
Nofuentes, G., Gueymard, C., Aguilera, J., Pérez-Godoy, M., Charte, F., 2017. Is the average photon energy a unique characteristic of the spectral distribution of global irradiance? Sol. Energy 149, 32–43.
Norton, M., Amillo, A.G., Galleano, R., 2015. Comparison of solar spectral irradiance measurements using the average photon energy parameter. Sol. Energy 120, 337–344.
Oreopoulos, L., Mlawer, E., Delamere, J., Shippert, T., Cole, J., Fomin, B., Iacono, M., Jin, Z., Li, J., Manners, J., et al., 2012. The continual intercomparison of radiation codes: Results from phase I. J. Geophys. Res.: Atmos. 117 (D6).
Perez, R., Ineichen, P., Seals, R., Michalsky, J., Stewart, R., 1990. Modeling daylight availability and irradiance components from direct and global irradiance. Sol. Energy 44 (5), 271–289.
Seity, Y., Brousseau, P., Malardel, S., Hello, G., Bénard, P., Bouttier, F., Lac, C., Masson, V., 2011. The AROME-France convective-scale operational model. Mon. Weather Rev. 139 (3), 976–991.
Singh, P., Ravindra, N.M., 2012. Temperature dependence of solar cell performance – an analysis. Sol. Energy Mater. Sol. Cells 101, 36–45.
Sjerps-Koomen, E., Alsema, E., Turkenburg, W., 1996. A simple model for PV module reflection losses under field conditions. Sol. Energy 57 (6), 421–432.
Skoplaki, E., Boudouvis, A., Palyvos, J., 2008. A simple correlation for the operating temperature of photovoltaic modules of arbitrary mounting. Sol. Energy Mater. Sol. Cells 92 (11), 1393–1402.
Stamnes, K., Tsay, S.-C., Wiscombe, W., Jayaweera, K., 1988. Numerically stable algorithm for discrete-ordinate-method radiative transfer in multiple scattering and emitting layered media. Appl. Opt. 27 (12), 2502–2509.
Stark, C., Theristis, M., 2015. The impact of atmospheric parameters on the spectral performance of multiple photovoltaic technologies. In: Photovoltaic Specialist Conference (PVSC), 2015 IEEE 42nd. IEEE, pp. 1–5.